Int. J. Heat Mass Transfer. Vol. 36, No. 3, pp. 543–552, 1993
Printed in Great Britain

0017-9310/93 $6.00 + 0.00

Entrance pipe flow and heat transfer for a Bingham plastic

GEORGE C. VRADIS,† JOHN DOUGHER‡ and SUNIL KUMAR†

†Department of Mechanical and Industrial Engineering, Polytechnic University, 333 Jay Street, Brooklyn, NY 11201, U.S.A.

‡GPU Nuclear Corporation, One Upper Pond Road, Parsippany, NJ 07054, U.S.A.

(*Received* 25 *March* 1992 *and in final form* 20 *May* 1992)

Abstract—The problem of the simultaneous development of the hydrodynamic and thermal fields in the entrance region of a circular pipe for a non-Newtonian Bingham-type fluid is solved numerically using the fully elliptic governing continuity, momentum and energy equations. A simultaneous variable solution technique for the system of finite difference equations is employed which has already been proven to efficiently and accurately predict Newtonian flows. Laminar flow and constant fluid properties are assumed. The solutions obtained are for a wide range of Reynolds, Yield, Prandtl and Brinkman numbers and are compared with other existing solutions based on reduced forms of the governing equations.

INTRODUCTION

A LARGE number of the fluids used extensively in industrial applications are fluids exhibiting a yield stress τ_0, that is a stress that has to be exceeded before the fluid moves. As a result such fluids cannot sustain a velocity gradient unless the magnitude of the local shear stress is higher than this yield stress. Fluids that belong to this category include cement, drilling mud, sludge, grease, granular suspensions, aqueous foams, slurries, paints, food products, plastics and paper pulp. The rheological behavior of a significant number of these fluids can be described by the constitutive equation for a Bingham plastic [1].

Given the wide occurrence of such flows, a detailed knowledge of their flow characteristics is of interest. The entrance flow problem in a circular pipe is of particular importance since it is encountered practically in every piping system. The initial effort in solving the hydrodynamic problem for Bingham fluids employed the integral boundary layer technique to obtain approximate solutions, as typified by the solutions of Chen *et al.* [2]. The appearance of the digital computer allowed the employment of numerical solutions for the boundary layer equations that provided increased accuracy and resolution, as described by Soto and Shah [3]. The corresponding heat transfer problem has been solved only for the case of the hydrodynamically fully developed flow using the boundary layer formulation for the temperature field (Graetz problem), as described by Wissler and Schechter [4] and Blackwell [5]. In a recent paper, Johnston [6] solved the Graetz problem including axial conduction and concluded that the Peclet number has to be greater than 1000 in order for the axial conduction term to be excluded without loss of accuracy. Forrest and Wilkinson [7] have also solved the Graetz problem with the additional effect of temperature dependent plastic viscosity. No solution for the simultaneously developing hydrodynamic and temperature fields has been reported in the literature.

The solution of the simultaneously developing hydrodynamic and temperature fields in the entrance region of a straight pipe for Newtonian fluids, as given by McDonald *et al.* [8] and Bentson and Vradis [9], shows that in the region close to the inlet of the pipe the boundry layer equations completely fail to predict the actual characteristics of the flow. While the boundary layer equations assume uniform pressure along each cross-section, the actual flow field exhibits strong transverse pressure gradients. In addition, close to the inlet a region of adverse pressure gradient exists. From these solutions, it is known that the full elliptic equations are needed to predict accurately the flow characteristics in the inlet region.

There are no results reported in the literature that employ the full elliptic equations for the solution of both the hydrodynamic and thermal entrance flow problem in a straight circular pipe for a Bingham fluid. In the present study a fully second-order accurate finite-difference formulation of the governing elliptic equations for mass conservation, momentum balance and energy conservation is used to solve this problem. A simultaneous variable solution technique is employed to solve the resulting system of non-linear equations which are linearized by employing an iterative marching solution procedure. The results obtained are compared with those obtained by the reduced forms of the governing equations. It is shown that substantial differences exist between these approximate solutions and the ones obtained in this study, and that the approximate solutions fail to predict many important features of the flow field.

THE GOVERNING EQUATIONS

The non-dimensionalized governing equations for the two-dimensional, steady, laminar, incompressible

NOMENCLATURE

Br	Brinkman number, $\mu U_i^2/k(T_i-T_w)$
C_f	friction coefficient, $\tau_w/\rho U_i^2$
D_w	diameter of pipe
h	heat transfer coefficient based on bulk temperature
k	thermal conductivity
Nu	Nusselt number, hD_w/k
Pr	Prandtl number, η/α
Pe	Peclet number, $Re\,Pr$
p	non-dimensional pressure, $P/\rho U_i^2$
P	pressure
r	non-dimensional radial distance, R/R_w
r_0	non-dimensional 'core' radius, R_0/R_w
R	radial distance
R_0	radius of the 'core'
R_w	radius of the pipe
Re	Reynolds number, $\rho U_i D_w/\eta$
T	temperature
u	non-dimensional streamwise velocity, U/U_i
U	streamwise velocity
v	non-dimensional radial velocity, V/U_i
V	radial velocity
x	non-dimensional streamwise distance, X/R_w
X	streamwise distance
Y	Yield number, $\tau_0 R_w/\eta U_i$.

Greek symbols

α	thermal diffusivity
Δ	rate of deformation tensor, $\Delta_{ij}=\partial u_i/\partial x_j+\partial u_j/\partial x_i$
η	plastic viscosity
θ	non-dimensional temperature, $(T-T_w)/(T_i-T_w)$
μ	effective viscosity
μ_{eff}	non-dimensional effective viscosity, μ/η
ρ	density
τ	stress tensor
τ_0	yield stress.

Subscripts

i	inlet
w	wall.

flow of a non-Newtonian fluid in cylindrical coordinates are:

$$\frac{\partial u}{\partial x}+\frac{1}{r}\frac{\partial rv}{\partial r}=0 \tag{1}$$

$$u\frac{\partial u}{\partial x}+v\frac{\partial u}{\partial r}=-\frac{\partial p}{\partial x}+\frac{1}{Re}\left[\frac{\partial}{\partial x}\left[2\mu_{eff}\frac{\partial u}{\partial x}\right]+\frac{1}{r}\frac{\partial}{\partial r}\left[\mu_{eff}r\left[\frac{\partial u}{\partial r}+\frac{\partial v}{\partial x}\right]\right]\right] \tag{2}$$

$$u\frac{\partial v}{\partial x}+v\frac{\partial v}{\partial r}=-\frac{\partial p}{\partial r}+\frac{1}{Re}\left[\frac{1}{r}\frac{\partial}{\partial r}\left[r2\mu_{eff}\frac{\partial v}{\partial r}\right]+\frac{\partial}{\partial x}\left[\mu_{eff}\left[\frac{\partial u}{\partial r}+\frac{\partial v}{\partial x}\right]\right]\right] \tag{3}$$

$$u\frac{\partial\theta}{\partial x}+v\frac{\partial\theta}{\partial r}=\frac{1}{Pe}\left[\frac{\partial^2\theta}{\partial x^2}+\frac{1}{r}\frac{\partial}{\partial r}\left[r\frac{\partial\theta}{\partial r}\right]\right]+\frac{Br}{Pe}\mu_{eff}\Phi, \tag{4}$$

where

$$\Phi=2\left[\left[\frac{\partial v}{\partial r}\right]^2+\left[\frac{v}{r}\right]^2+\left[\frac{\partial u}{\partial x}\right]^2\right]+\left[\frac{\partial v}{\partial x}+\frac{\partial u}{\partial r}\right]^2. \tag{4a}$$

In the case of a Bingham fluid the relationship between the stress tensor τ and the rate of deformation tensor Δ is given by the following formula [1]:

$$\tau=\left\{\eta+\frac{\tau_0}{\sqrt{(1/2(\Delta:\Delta))}}\right\}\Delta \quad \text{for} \quad (\tau:\tau)>2\tau_0^2$$

$$\Delta=0 \quad \text{for} \quad (\tau:\tau)\leqslant 2\tau_0^2. \tag{5a, b}$$

Here $\Delta:\Delta=\sum_i\sum_j\Delta_{ij}\Delta_{ji}$ is the second invariant of Δ. Equation (5a) is valid in the case of the shear stresses. Additional higher order terms which are a function of the corotational derivative of Δ and of the single dot product of Δ with itself, have to be added in equation (5a) to describe accurately the normal stresses. No systematic experimental and/or theoretical study of the importance of these higher order terms in describing such flow fields exists. These higher order terms are neglected in the present study. In cylindrical coordinates the function $1/2(\Delta:\Delta)$ is given by

$$\tfrac{1}{2}(\Delta:\Delta)=2\left[\left[\frac{\partial v}{\partial r}\right]^2+\left[\frac{v}{r}\right]^2+\left[\frac{\partial u}{\partial x}\right]^2\right]+\left[\frac{\partial v}{\partial x}+\frac{\partial u}{\partial r}\right]^2. \tag{5c}$$

As a result the non-dimensional effective viscosity is defined as

$$\mu_{eff}=\left\{1+\frac{Y}{\sqrt{(1/2(\Delta:\Delta))}}\right\} \quad \text{for} \quad (\tau:\tau)>2\tau_0^2 \tag{6a}$$

$$\mu_{eff}=\infty \quad \text{for} \quad (\tau:\tau)\leqslant 2\tau_0^2 \tag{6b}$$

where $Y = \tau_0 R_w/\eta U_i$ is the Yield number for Bingham fluids. Equation (6) accurately expresses the effective viscosity associated with the shear stresses. However, because of the neglect of the higher order terms in equation (5a), equation (6) expresses the normal stresses only in an approximate manner.

THE SOLUTION TECHNIQUE

The numerical technique used in the present study is described in detail by Bentson and Vradis [9] and Vradis and VanNostrand [10], and has been shown to be both accurate and computationally efficient for Newtonian flows. It employs the well-known staggered grid proposed by Welch *et al.* [11] for the Marker and Cell method, in conjunction with a second-order accurate finite-differences formulation of the governing elliptic equations. The resulting system of non-linear algebraic equations is solved using an iterative procedure, in which the non-linearities are treated by using values from the previous iteration level (quasi-linearization). The effective viscosity is evaluated at the end of each iteration using the newly obtained velocity field. The linear algebraic equations are solved simultaneously along lines perpendicular to the main flow direction, marching from the inlet to the outlet of the pipe. The convergence parameter employed in the present analysis is the magnitude of the maximum residual in the difference equations. The discretization is made in such a way that the continuity equation is always satisfied to 'machine accuracy' at any stage of the solution procedure. Therefore, convergence is checked for the two momentum and energy equations and the iterative procedure is terminated when the residual in the non-dimensional equations become less than 10^4.

As is obvious from the governing equations, the only possible coupling of the momentum equations with the energy equation is through the viscosity. In the case where the viscosity is independent of temperature (as it is assumed to be in the present study), the hydrodynamic problem is completely independent of the thermal one. As a result, the continuity and momentum equations are solved first, simultaneously. Once the velocity field has been obtained to the desired level of accuracy, the energy equation, which is linear, is solved for the temperature distribution.

A 98×60 grid (in the axial and radial directions, respectively) was used which was non-uniform in the streamwise direction, increasing geometrically from the inlet to the outlet, and uniform in the transverse direction. The grids used in all cases gave grid independent solutions, with the exception of the first point downstream of the inlet where the predicted Nusselt number is extremely sensitive to the grid due to the mathematical singularity imposed by the boundary conditions at that point.

As seen from equations (6a) and (6b) the effective viscosity μ_{eff} attains an infinite value when $\Delta : \Delta = 0$. Large values of μ_{eff} generate computational difficulties since the coefficient matrix is rendered very 'stiff', thus resulting in lack of convergence. Therefore, when the value of $\Delta : \Delta$ drops below a certain level the effective viscosity μ_{eff} is 'frozen' at a certain high value in order to guarantee convergence. Different levels of upper values for the effective viscosity were investigated for their accuracy and computational efficiency. The results were shown to be quite insensitive of this high cut off value once it exceeded a value of about 500. A value of 1000 was adopted. This, in conjunction with a strong under-relaxation of the viscosity coefficient (of the order of 50–99%, depending on the Yield number), proved to offer the best combination for numerical accuracy and computational efficiency.

RESULTS

The geometry and the boundary conditions of the problem are shown in Fig. 1. The flow at the inlet ($x = 0$) is assumed to be uniform ($u = 1, v = 0$), as is the temperature ($\theta = 1$). At the exit the flow is assumed fully developed, both hydrodynamically and thermally, allowing the streamwise derivatives of the velocities and the temperature to be set to zero, while the pressure remains uniform. It is always verified after every run that the downstream boundary was located far enough from the inlet so that the flow there was completely fully developed. The length of the computational domain depends on the Reynolds, Prandtl and Yield numbers and since it is not known a priori, it is adjusted according to the above. As an example, in the case of $Re = 5$, $Pr = 0.1$ and $Y = 1$, the length of the domain is 6 pipe diameters, while in the case of $Re = 50$, $Pr = 10$, $Y = 1$ the length is 13 pipe diameters. Along the solid walls ($r = 1$) the velocities satisfy the no-slip condition ($u = v = 0$), while the non-dimensional temperature vanishes ($\theta = 0$).

The convergence rate of the numerical scheme is strongly influenced by the Yield number Y. Figure 2 shows the convergence history for the hydrodynamic problem for $Re = 50$ and a 98×60 grid for four different Yield numbers ($Y = 0$, 2, 5 and 10). For a fixed grid size and Reynolds number, the higher Yield number cases require a larger number of iterations for convergence to the same accuracy level. This is due to the increased 'stiffness' of the coefficient matrix as indicated previously. For the higher Yield numbers convergence is obtained only after using very strong under-relaxation of the effective viscosity (of the order

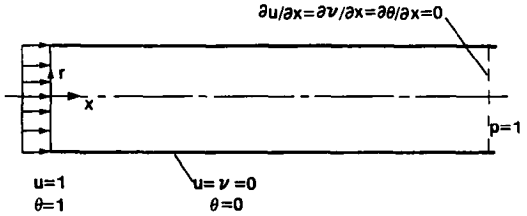

FIG. 1. Geometry and boundary conditions.

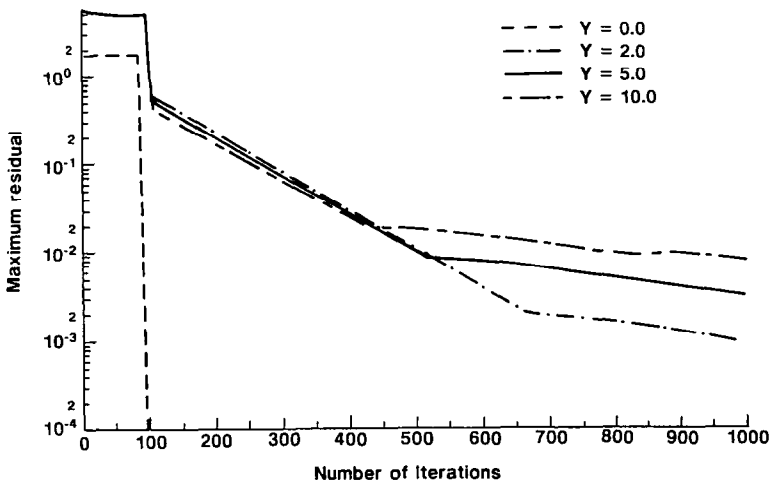

FIG. 2. Convergence history for different Yield numbers (98 × 60 grid).

of 95–99%). In these cases the number of iterations required to reach the prescribed residual level of 10^{-4} was of the order of 4000–5000. Typically 20–30 iterations are required for the temperature solution to be obtained to the desired level of accuracy. A number of different acceleration schemes have been reported in the literature to increase the convergence rate of algorithms like the one employed in the present study. Their incorporation here would probably substantially reduce the number of iterations required and are the subject of on-going research.

The accuracy of the solution procedure is established by comparing the numerical results obtained for the velocity profile in the fully developed flow region with those predicted by the available exact analytical solution [12] of the governing equations in this region. The results for different values of Yield number are shown in Fig. 3. As seen, the numerical results are within less than 1% of the analytic solutions. The small deviations are due to the finite value assigned to the effective viscosity in the 'core' region (where the actual value of $\mu_{\text{eff}} = \infty$) in order to guarantee convergence. The higher the upper limit value for the effective viscosity is, the smaller are the deviations between the two solutions. As expected, the fact that the effective viscosity in the core region is not infinite in the present calculation results in a core region with a non-perfectly uniform velocity distribution. The velocity decreases slightly within this region as the radial distance increases. An interesting feature of this solution is the fact that the velocity gradient at the wall is much less sensitive than that at the centerline to the 'cut off' effective viscosity. This is highly desirable given that most of the phenomena of interest to engineering practice are boundary phenomena.

Figures 4–6 show developing velocity profiles for $Re = 50$ and $Y = 0$, 2, 5 and 10, respectively, at different distances from the inlet. The velocity overshoots present in the Newtonian flow solutions

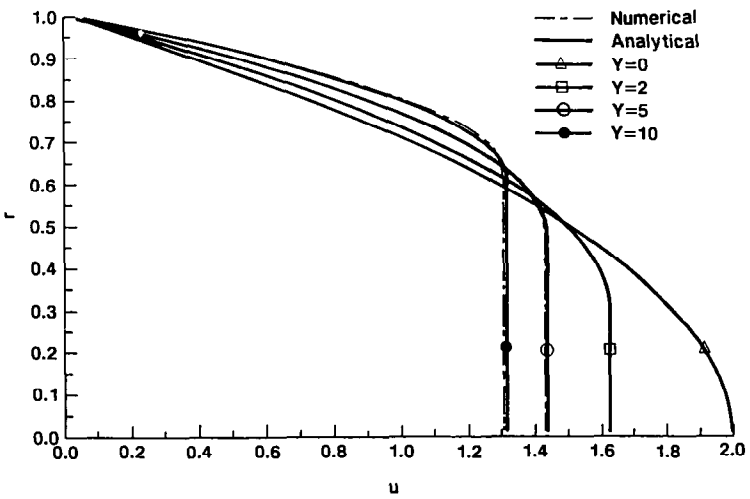

FIG. 3. Fully developed velocity profiles.

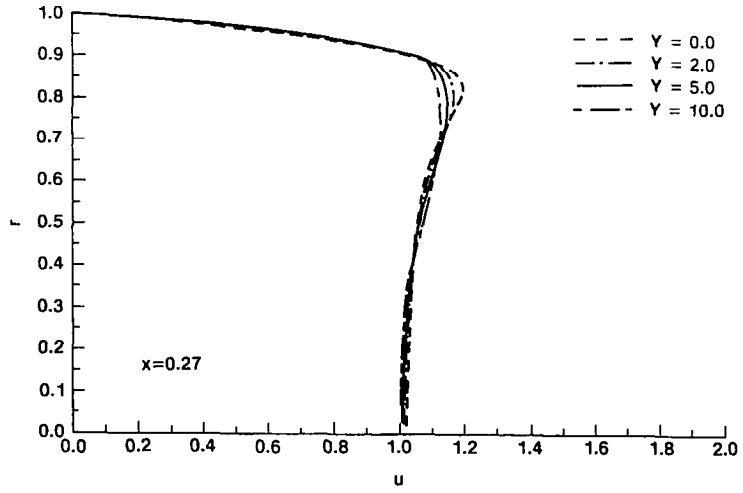

FIG. 4. Developing velocity profiles for $Re = 50$, $Y = 0, 2, 5$ and 10 at $x = 0.27$.

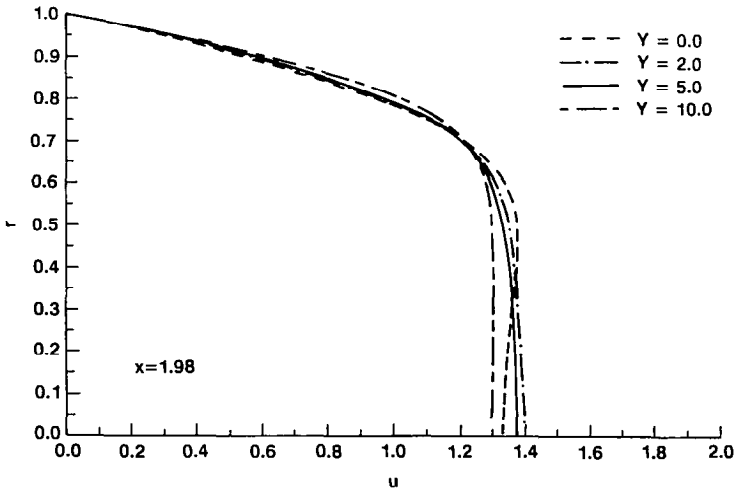

FIG. 5. Developing velocity profiles for $Re = 50$, $Y = 0, 2, 5$ and 10 at $x = 1.98$.

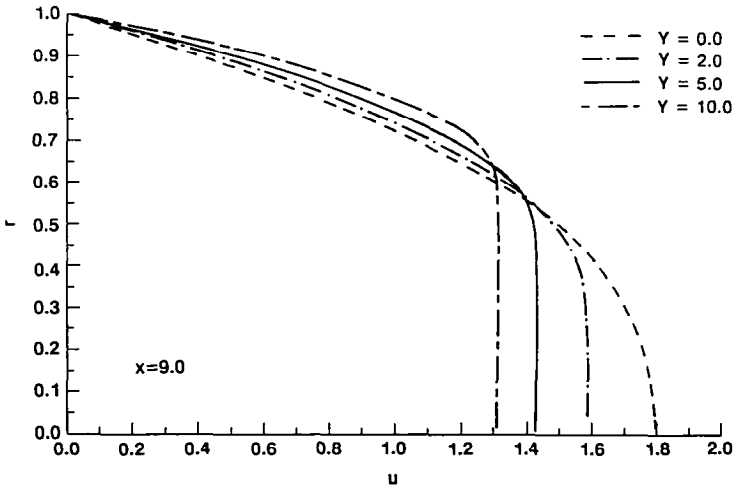

FIG. 6. Developing velocity profiles for $Re = 50$, $Y = 0, 2, 5$ and 10 at $x = 9.0$.

($Y = 0$) in the region close to the inlet are characteristic of fully elliptic solutions and not predicted by any reduced form of the equations such as partially parabolized Navier–Stokes or boundary layer formulations [9]. As seen in Figs. 4–6, the same overshoots are present in the flow of non-Newtonian Bingham fluids. A common point of confusion in the analysis of flow behavior of Bingham fluids is the association of any point of inflection in the velocity profile ($\partial u/\partial r = 0$) with the presence of a 'core' flow region. Such association is valid only in pure shear flows, such as those that have been the subject of previous investigations [6, 7]. In the flow situation encountered in the present study, the inflection point in the developing velocity profiles does not result in 'core' flow regions. This is due to the non-zero value of the rest of the terms in equation (5c), which makes the value of $\Delta : \Delta$ different than zero. As these figures demonstrate, the velocity overshoots are dampened by increasing Yield numbers eventually disappearing as plug flow ($Y = \infty$) is asymptotically approached. It is also noted that the velocity profiles develop faster with higher values of the Yield number. This is to be expected, given the increase of the core radius with the Yield number.

The developing centerline velocity is given in Fig. 7 for $Re = 50$ and $Y = 0, 2, 5$ and 10. In the region very near to the inlet, the centerline velocity develops faster for lower Yield numbers. After that, as the Yield number increases, the slope of the curve increases. Thus, the velocity develops faster and as a result the entrance length decreases as the Yield number increases. It should be mentioned here that if the maximum value of the effective viscosity employed is reduced below a certain limit, centerline velocity overshoots appear right before fully developed conditions are established. These overshoots become profound in the case of small upper limits for μ_{eff} and cannot be eliminated through grid refinement. The results obtained in this study are compared to those of Chen *et al.* [2] who employed an integral boundary layer technique. As seen for the two cases compared ($Y = 2$ and 5) the solutions are fundamentally different. The boundary layer solutions, unable to predict the adverse pressure gradients present in the inlet region, allow for the rapid growth of the centerline velocity in that region. Consequently, the corresponding high friction factors associated with the entrance region are severely under-predicted.

Figure 8 shows the variation of the friction coefficient C_f along the pipe wall with streamwise distance, again for $Re = 50$ and different Yield numbers. As expected, the entrance region is associated with friction coefficients substantially higher than those in the fully developed flow region. Throughout the pipe the friction coefficient increases with the Yield number due to increased velocity gradients along the pipe wall imposed on the flow by the increased size of the core region. Therefore, the corresponding friction factors are increasing with increasing Yield numbers.

Figure 9 shows the effect of the Yield number on the streamwise Nusselt number distributions for $Re = 50$, $Pr = 1$ and $Br = 0$. In the fully developed region the Nusselt number increases with the Yield number due to the greater heat removal rate by the higher velocity gradients at the wall. It is very important to notice here that in the entrance region an increase in the Yield number results in a minimal increase in the corresponding Nusselt number. This behavior is similar to that observed in the analytical solution of the boundary layer equations (Graetz problem) in ref. [5], where a hydrodynamically fully developed flow is assumed. In the present case however, the corresponding Nusselt numbers at the inlet are higher than those in the Graetz problem given the higher velocity gradients at the wall associated with a hydrodynamically developing flow.

Figure 10 shows the Nusselt number variation with

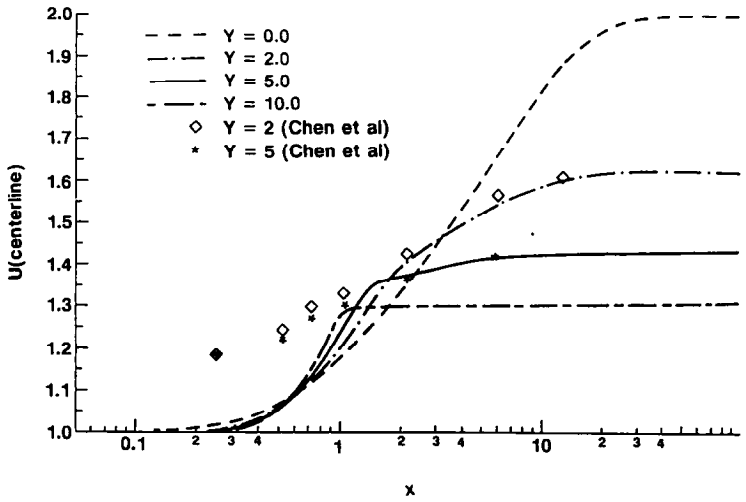

FIG. 7. Developing centerline velocity profiles for $Re = 50$.

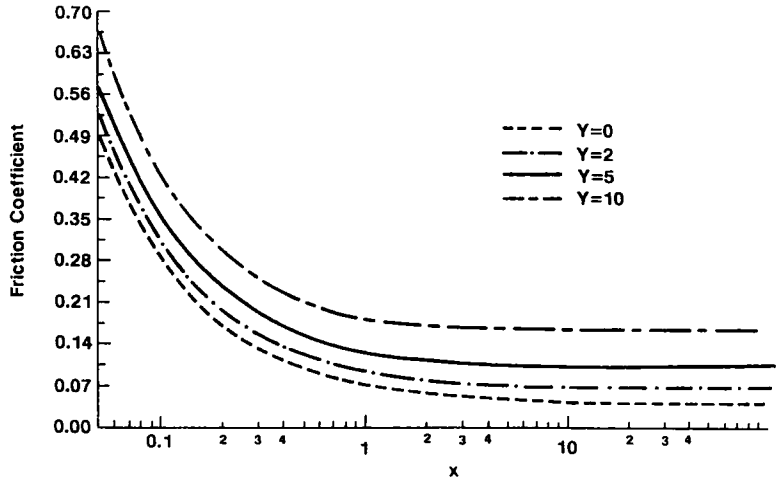

FIG. 8. Friction coefficient vs streamwise distance for $Re = 50$.

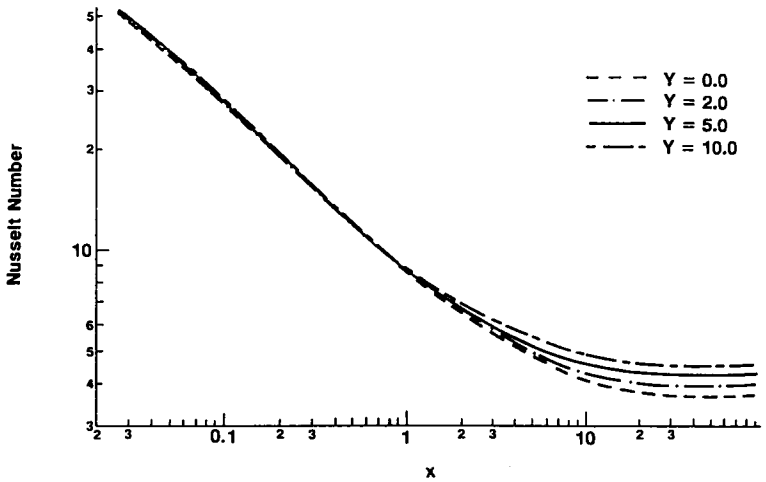

FIG. 9. Nusselt number vs streamwise distance for $Re = 50$, $Pr = 1$ and $Br = 0$.

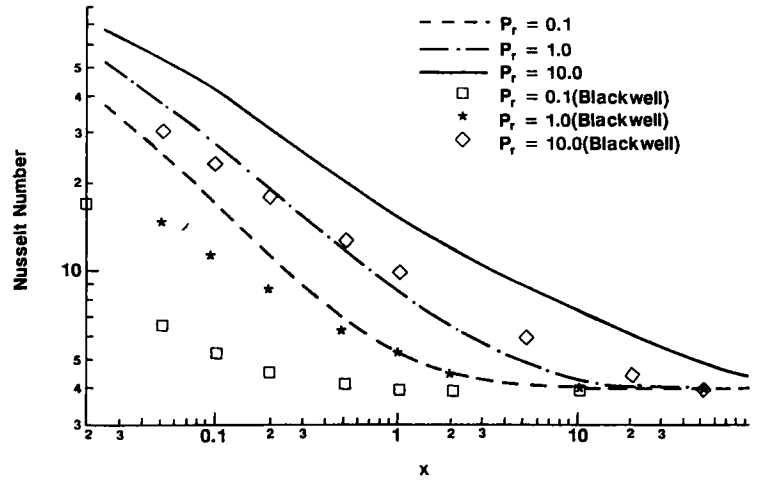

FIG. 10. Nusselt number vs streamwise distance for $Re = 50$, $Y = 2$ and $Br = 0$.

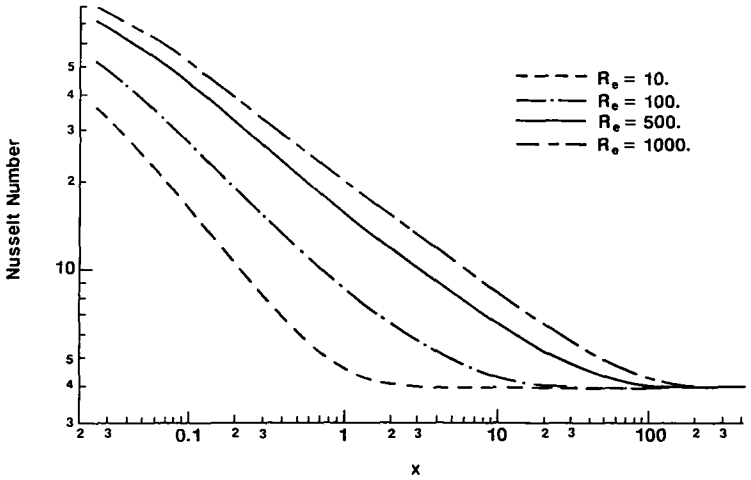

FIG. 11. Nusselt number vs streamwise distance for $Pr = 1$, $Y = 2$ and $Br = 0$.

streamwise distance for $Re = 50$, $Y = 2$, $Br = 0$ and for $Pr = 0.1$, 1.0 and 10.0. As seen, higher Prandtl numbers are associated with higher inlet Nusselt numbers and longer thermal entrance lengths, as the case with Newtonian fluids. The results obtained in this study are compared to those by Blackwell [5] where a hydrodynamically fully developed flow is assumed and the axial conduction terms are neglected. Very substantial quantitative differences exist between the two solutions in the entrance region, the results in ref. [5] giving much smaller values. Again, this is due to the assumption of hydrodynamically fully developed flow, which eliminates the entrance region with its sharp velocity gradients and corresponding higher heat transfer rates. For the low Prandtl number cases ($Pr = 0.1$) the differences close to the inlet are of one order of magnitude. In the fully developed flow region the two solutions are identical, as expected.

Figure 11 shows the effect of the Reynolds number on the streamwise Nusselt number distribution for $Pr = 1$, $Y = 2$ and $Br = 0$. As expected, the higher the Reynolds number, the higher the Nusselt number at the inlet and the larger the thermal entrance length. As the fully developed flow condition is approached the Nusselt number asymptotically reaches the same value independently of the Reynolds number, since the fully developed velocity profile and the core size depend on the Yield number only.

In the case of Newtonian fluids viscous heating effects are usually negligible, unless high speeds are present. The same cannot be said in the case of non-Newtonian fluids where such effects play a predominant role in determining the heat transfer characteristics of the flow even at relatively low speeds. Again, in order to establish the accuracy of the numerical calculations once more, the effect of the Brinkman number on the heat transfer for a Newtonian fluid was studied and the numerical results were compared to the exact solution of the governing equations in the fully developed flow regime. The agreement was excellent.

Figure 12 shows the effect of the Brinkman number

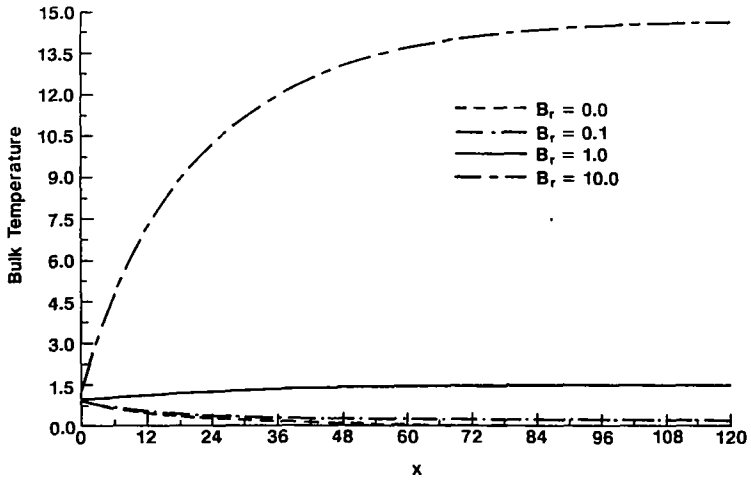

FIG. 12. Bulk temperature vs streamwise distance for $Re = 50$, $Y = 5$ and $Pr = 1$.

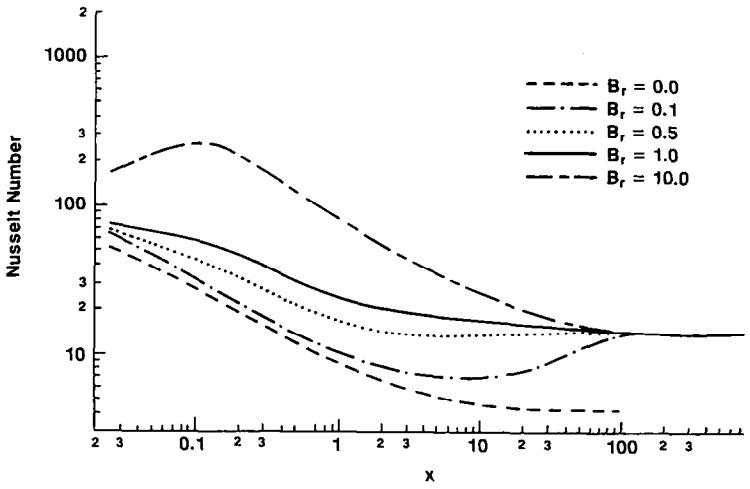

FIG. 13. Nusselt number vs streamwise distance for $Re = 50$, $Y = 5$ and $Pr = 1$.

on the bulk temperature for $Re = 50$, $Y = 5$ and $Pr = 1$. As seen, the effect is profound. Due to the dissipation of mechanical energy into heat the fluid temperature in the fully developed flow region is higher than that of the wall. In the fully developed flow regime the analytical solution for the temperature distribution can be obtained by integrating the governing equations. This solution has not been reported in the literature and so it is given here in the Appendix. The agreement between the analytical and computational results is excellent, the differences being not distinguishable on figures, therefore they are not presented here. As fully developed flow conditions are approached, the bulk temperature reaches its asymptotic value which is a linear function of the Brinkman number only. Notice that for a Brinkman number greater than about one the fluid is heated instead of cooled due to the excessive dissipation of mechanical energy to heat.

Figure 13 shows the effect of the Brinkman number on the Nusselt number for $Re = 50$, $Y = 5$ and $Pr = 1$. The Nusselt number in the thermally fully developed region (based on the bulk temperature) depends on the Yield number only and is independent of the Brinkman number. Again, the temperature gradients at the wall obtained from the analytical solution in the fully developed flow region were compared with the numerical results and the agreement is excellent. In the entrance region, as the Brinkman number increases the Nusselt number increases sharply, resulting in order of magnitude differences in heat transfer rates. It is also noted here that the rate of decrease of the Nusselt number in the very near entry region decreases with increasing Brinkman numbers and that eventually at very high values of the Brinkman number, the Nusselt number actually increases, thus exhibiting a local maximum downstream of the inlet. There are two competing mechanisms here. One is the growth of the hydrodynamic and thermal boundary layers close to the inlet, which results in decreasing gradients at the wall and consequently lower Nusselt numbers. The second is the increase in the bulk temperature of the fluid due to the dissipation of mechanical energy to heat, which results in increased temperature differences and consequently higher Nusselt numbers. As seen, for Br slightly above one the Nusselt profile at the inlet is very close to being flat, indicating that the two mechanisms in this case are practically balancing each other. Further downstream as the bulk temperature reaches its asymptotic value and the flow tends toward fully developed conditions, the Nusselt number drops to its asymptotic value.

CONCLUSIONS

The problem of the simultaneous development of the hydrodynamic and thermal fields in the entrance region of a straight circular pipe for the laminar flow of a non-Newtonian Bingham fluid has been solved numerically. A finite-difference second-order accurate scheme has been employed in conjunction with a marching iterative solution technique. To the authors' best knowledge this is the first reported solution of elliptic Bingham fluid flows employing a finite-differences scheme. The successful completion of this work indicates that such schemes, which are the most widely used ones in fluid flow and heat transfer calculations for Newtonian fluids, in conjunction with advanced solution techniques, can be adopted for the solution of complicated highly non-linear non-Newtonian flows with success.

It has been shown that fully elliptic numerical solutions are required to accurately predict the flow field of non-Newtonian Bingham-type fluids in the entrance region. Such solutions have not been reported in the literature and are presented here. As is the case for Newtonian fluids, Bingham fluids exhibit velocity overshoots in the entrance region of the pipe, the overshoots diminishing with increasing Yield numbers. The present analysis has also demonstrated

the strong influence of the Yield number on the hydrodynamic and heat transfer characteristics of this flow. One exception is the weak dependence of the Nusselt number in the entrance region on the Yield number. In addition, the effects of the Brinkman number are very important, resulting in Nusselt numbers with an order of magnitude higher than those in which viscous dissipation effects are neglected, even for moderate values of the Brinkman number.

REFERENCES

1. R. B. Bird, W. E. Stewart and E. N. Lightfoot, *Transport Phenomena*, pp. 103–104. Wiley, New York (1960).
2. S. S. Chen, L. T. Fan and C. L. Hwang, Entrance region flow of the Bingham fluid in a circular pipe, *A.I.Ch.E. Jl* **16,** 293–299 (1970).
3. R. J. Soto and V. L. Shah, Entrance flow of a yield-power law fluid, *Appl. Sci. Res.* **32,** 73–85 (1976).
4. E. H. Wissler and R. S. Schechter, The Graetz–Nusselt problem (with extension) for a Bingham plastic, *Chem. Engng Prog. Symp. Series 29* **55,** 203–208 (1959).
5. B. F. Blackwell, Numerical solution of the Graetz problem for a Bingham plastic in laminar tube flow with constant wall temperature, *J. Heat Transfer* **107,** 466–468 (1985).
6. P. R. Johnston, Axial conduction and the Graetz problem for a Bingham plastic in laminar tube flow, *Int. J. Heat Mass Transfer* **34,** 1209–1217 (1991).
7. G. Forrest and W. L. Wilkinson, Laminar heat transfer to temperature-dependent Bingham fluids in tubes, *Int. J. Heat Mass Transfer* **16,** 2377–2391 (1973).
8. J. W. McDonald, V. E. Denny and A. F. Mills, Numerical solutions of the Navier–Stokes equations in inlet regions, *J. Appl. Mech.* **94,** 873–878 (1972).
9. J. Bentson and G. Vradis, A two-stage pressure correction technique for the incompressible Navier–Stokes equations, AIAA Paper 87-0545, 25th Aerospace Sciences Meeting, 12–15 January (1987).
10. G. Vradis and L. VanNostrand, Laminar coupled flow downstream of an asymmetric sudden expansion, *AIAA J. Thermophys. Heat Transfer* **6,** 288–295 (April–June 1992).
11. J. E. Welch, W. H. Harlow, J. P. Shannon and B. J. Daly, The MAC method, Report LA-3425, Los Alamos Scientific Lab (1966).
12. R. B. Bird, R. C. Armstrong and O. Hassager, *Dynamics of Polymeric Liquids*, Vol. 1, p. 264. Wiley, New York (1977).

APPENDIX

The problem of the steady, fully developed, laminar flow in a circular pipe with viscous heating for a Bingham fluid has not been reported in the literature and for this reason it is given in this Appendix.

In the case of a Bingham fluid, the non-dimensionalized governing equations describing the flow are

$$u = \frac{1}{2}\frac{Y}{r_0}(1-r^2) - Y(1-r) \quad \text{for} \quad r_0 \leqslant r \leqslant 1 \tag{A1a}$$

$$u = \frac{1}{2}\frac{Y}{r_0}(1-r_0^2) - Y(1-r_0) \quad \text{for} \quad 0 \leqslant r \leqslant r_0 \tag{A1b}$$

and

$$\frac{1}{r}\frac{\mathrm{d}}{\mathrm{d}r}\left[r\frac{\mathrm{d}\theta}{\mathrm{d}r}\right] = -Br\,\mu_{\mathrm{eff}}\Phi = -Br\,\mu_{\mathrm{eff}}\left[\frac{\mathrm{d}u}{\mathrm{d}r}\right]^2 \tag{A2}$$

where

$$\mu_{\mathrm{eff}} = 1 + \frac{Y}{\left|\frac{\mathrm{d}u}{\mathrm{d}r}\right|} \quad \text{for} \quad r_0 < r \leqslant 1 \tag{A3a}$$

$$\mu_{\mathrm{eff}} = \infty \quad \text{for} \quad 0 \leqslant r \leqslant r_0. \tag{A3b}$$

Integrating equation (A2) once, using equations (A1) and (A3), the temperature gradient is obtained as

$$\frac{\mathrm{d}\theta}{\mathrm{d}r} = -Br\frac{Y^2}{r_0^2}\left[\frac{r^3}{4} - r_0\frac{r^2}{3}\right] - Br\frac{Y^2}{12}\frac{r_0^2}{r}. \tag{A4}$$

The temperature gradient at the wall then is

$$\left[\frac{\mathrm{d}\theta}{\mathrm{d}r}\right]_{\mathrm{w}} = Br\frac{Y^2}{12r_0^2}[-r_0^4 + 4r_0 - 3]. \tag{A5}$$

For a Newtonian fluid ($Y = 0$), $Y/r_0 = 4$, therefore $[\mathrm{d}\theta/\mathrm{d}r]_{\mathrm{w}} = -4Br$, which is the exact solution in that case. Integrating equation (A5) over r, and setting $\theta = 0$ at the wall, the following expression is obtained for the temperature distribution:

$$\theta(r) = Br\left[\frac{Y}{16r_0^2}(1-r^4) - \frac{Y^2}{9r_0}(1-r^3) - \frac{Y^2r_0^2}{12}\ln r\right]$$
$$\text{for} \quad r_0 \leqslant r < 1 \tag{A6a}$$

$$\theta(r) = \theta_0 = Br\left[\frac{Y^2}{16r_0^2}(1-r_0^4) - \frac{Y^2}{9r_0}(1-r_0^3) - \frac{Y^2r_0^2}{12}\ln r\right]$$
$$\text{for} \quad 0 < r < r_0. \tag{A6b}$$

In the case of a Newtonian fluid $\theta = \theta_0 = Br$, which is obtained for $Y/r_0 = 4$ and which is the exact solution in that case.